

Contents List available at JACS Directory

Journal of Advanced Chemical Sciences

journal homepage: www.jacsdirectory.com/jacs



Removal of As(III) from Aqueous Solution using Zinc Oxide Nanoparticle Embedded on Activated Silica and ANN Modeling

D. Gnanasangeetha^{1,*}, D. Sarala Thambavani²

- ¹Department of Chemistry, PSNA College of Engineering & Technology, Dindigul 624 622, TN, India.
- ²Research and Development Centre, Bharathiar University, Coimbatore 641 046, TN, India.

ARTICLE DETAILS

Article history:
Received 02 February 2015
Accepted 10 February 2015
Available online 15 February 2015

Keywords:
Artificial Neural Network
Adsorption
Arsenic
Back Propagation Algorithm
Levenberg-Marquardt Algorithm

ABSTRACT

In the present work removal of arsenic from aqueous solution using zinc oxide nanoparticle embedded on activated silica as adsorbent was studied. The initial As(III) concentration was varied from 0.01N to 0.1N with varying amount of zinc oxide nanoparticle embedded onto activated silica $1-8\,g$ in laboratory batch adsorption experiment. The maximum adsorption efficiency was found at As(III) initial concentration of 0.06 N, adsorption dose of 8 g/L and pH of the solution of 5.0. The equilibrium contact time was found at 100 min. A three layer feed forward artificial neural network (ANN) with back propagation training algorithm was developed to model the adsorption process of As(III) in aqueous solution using Zinc oxide nanoparticle embedded onto activated silica as adsorbent. The neural network architecture consisted of tangent sigmoid transfer function at hidden layer with 10 hidden neurons, linear transfer function at output layer and Levenberg-Marquardt (LM) back propagation training algorithm. The neural network model predicted values are found in close agreement with the batch experiment result with correlation coefficient (R) of 0.999 and mean squared error (MSE) 4.39.

1. Introduction

Arsenic is naturally present at high levels in the groundwater of a number of countries. Arsenic is highly toxic in its inorganic form. Contaminated water used for drinking, food preparation and irrigation of food crops poses the greatest threat to public health from arsenic. Longterm exposure to arsenic from drinking-water and food can cause cancer and skin lesions [1-2]. Skin lesions and skin cancer are the most characteristic effects. The greatest threat to public health from arsenic originates from contaminated groundwater. People who smoke tobacco can also be exposed to the natural inorganic arsenic content of tobacco because tobacco plants essentially take up arsenic naturally present in the soil. Also in the past the potential for elevated arsenic exposure was much greater when tobacco plants used to be treated with lead arsenate insecticide [3-5]. The immediate symptoms of acute arsenic poisoning include vomiting, abdominal pain and diarrhea. These are followed by numbness and tingling of the extremities, muscle cramping and death in extreme cases. The International Agency for Research on Cancer (IARC) has classified arsenic and arsenic compounds as carcinogenic to humans and has also stated that arsenic in drinking-water is carcinogenic to humans. Other adverse health effects that may be associated with longterm ingestion of inorganic arsenic include developmental effects, neurotoxicity, diabetes and cardiovascular disease. The most important action in affected communities is the prevention of further exposure to arsenic by the provision of a safe water supply for drinking, food preparation and irrigation of food crops [4-7].

There are a number of options to reduce levels of arsenic in drinking-water. The present study is aimed at selection of a low cost adsorbent which can adsorb arsenic from aqueous solution. Detailed batch studies with the selected adsorbent, *Azadirachta indica, Corriandrum sativum, Acalypha indica, Ocimum sanctum* have been carried out in the earlier investigation. The tribulations of our bionetwork are increasing with the encroachment in technology [8-11]. Techniques used for deduction of heavy metals like lime coagulation, reverse osmosis, chemical precipitation, ion exchange and solvent extraction are expensive and non-environmental friendly as compared to adsorption. Adsorption is one of

the easiest safest and most expenditure effective methods for the removal of metals. The foremost advantage of an adsorption system of silica embedded zinc oxide nanoparticle are less investment in terms of both initial cost and simple designed easy operation and has no effect of toxic substance compared to conventional chemical treatment process. There is a vital requirement for development of innovative but low cost processes by which heavy metals can be removed. Adsorption technique is quite trendy due its simplicity and high efficiency, as well as the ease of use of a wide range of adsorbents [12-14]. Increasing awareness towards green chemistry and biological processes has led to the efficacy and feasibility of an eco-friendly approach for the synthesis of ZnO nanoparticle entrenched on activated silica as proficient adsorbent for removal of As(III) using Artificial Neural Network.

2. Experimental Methods

2.1 Adsorbent Preparation and Characterisation

Aqueous leaf extract of Emblica officinalis (Eo) was stirred for 30 min to that 1g of zinc acetate dihydrate was added under vigorous stirring. After 1hr stirring 10 g of activated silica was introduced into the above solution followed by the addition of aqueous NaOH resulted in a white aqueous solution at pH 12. This was then sited in a magnetic stirrer for 2hr. The activated silica (AS) supported ZnO nanoparticle (ZNO-NPS) using Emblica officinalis (Eo) were then filtered and washed with double distilled water. The synthesized zinc oxide nanoparticle embedded on activated silica (ZnO-NPs-AS-Eo) was maintained at 60 °C for 12 hrs. ZnO-NPs-AS-Eo structure was primed by green synthesis method. A mortar was used to homogeneously ground ZnO-NPs-Eo. The proposed sorbent were stored in air at room temperature. The X-Ray powder diffraction pattern of the as-synthesized sample was recorded on an X-ray diffractometer (XRD, PW 3040/60 Philips X'Pert) using Cu (K α) radiation (λ =1.5416Å) operating at 40 kv and 30 mA with 2θ ranging from 10-90°. Fourier transform infrared (FT-IR) spectra was recorded on Jasco FT-IR5300 model spectrophotometer in KBr pellets. The external morphology of the sample were characterized by scanning electron microscope (SEM) (LEO 1530FEGSEM).

*Corresponding Author

Email Address: sangithprakash@yahoo.co.in (D. Gnanasangeetha)

2.2 Biosorption Studies

Sorption studies using standard practices were carried out in batch experiments (duplicate) as a function of adsorbent dosage (0 - 8 g), contact time (20 - 130 min), volume of the test solution (20 - 250 mL), metal concentration (0.01 - 0.1 N), with pH (0 - 8) and agitation speed of (100 – 500 rpm). The details of methodology have been described in our earlier publications [2]. Percent metal uptake by the adsorbent has been computed using the following equation % Sorption = $(C_o - C_e)x100/C_o$, where C_o and C_e are the initial and final concentration of metal ions in the solution.

3. Results and Discussion

3.1. Adsorbent Characterisation

3.1.1. XRD Spectra of ZnO-NPs-AS-Eo

The experimental results show that significant rod shaped ZnO-NPs-AS is produced with distilled water as the reference environment with aqueous leaf extract of *Emblica officinalis*. The aqueous leaf extract of *Emblica officinalis*. The aqueous leaf extract of *Emblica officinalis* acts as a complexing template which prevents the particles formed from aggregating due to its physicochemical properties. XRD spectrum Fig. 1 shows distinctive peaks with (100), (002), (101), (110), (103), (200), (112) and (201) which confirms that the asynthesized material possess wurtzite hexagonal phase of ZnO nanoparticles. All the samples had favorite orientation along the (101) plane. The average crystalline sizes (D) of the nano-sized ZnO particles are fabricated from Table 1 and it is observed as 16 nm.

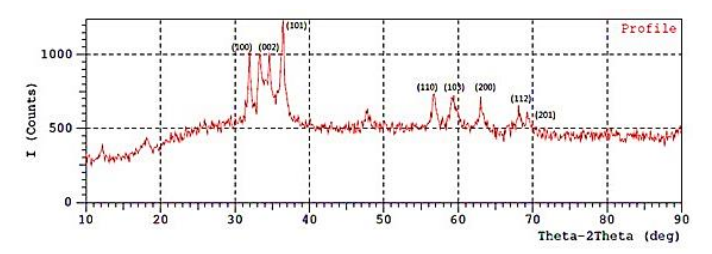


Fig. 1 XRD spectra of ZnO-NPs-AS-Eo

Table.1. Hexagonal wurtzite phase of ZnO nanoparticles

Strong Peaks (20)	(θ)	Planes hkl	Spacing (dhkl±0.0006)	FWHM	B (radian)	Crystallite size	Particle size (nm)	Morphology (shape)
33.4000	16.7000	100	0.2913	1.1562	0.0201	25.4	100	
34.5000	17.2500	002	0.3009	0.0000	0.0000	0.46	100	Nano rods
36.3135	18.1567	101	0.3163	1.0859	0.0189	23	100	

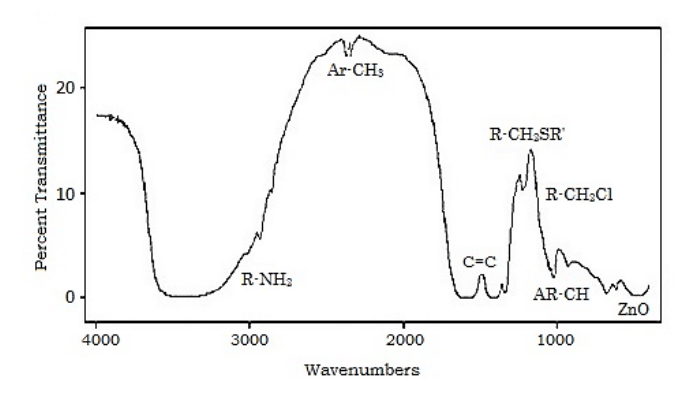


Fig. 2 FT-IR spectrum of ZnO-NPs-AS-Eo

3.1.2. Fourier Transform Infrared Spectroscopy (FT-IR)

FT-IR study of dry powdered test drug in KBR pellet was investigated to identify the presence of functional groups (Fig. 2). A clear ZnO stretching mode was observed at 417-557 cm⁻¹. The pattern of absorptions at 665 cm⁻¹ matches up aromatic C-H. Absorption peak at 930 cm⁻¹ point out the aromatic stretching (out of plane bending). Primary amine (R-NH2) show two N-H stretching bands in the range 3550-3300 cm⁻¹. Bands at 1015 cm⁻¹ ¹ symbolize the aromatic skeletal vibration. The corresponding CH₂ out of plane bending vibration characteristic of group RCH₂SR' and RCH₂Cl group appears at 1213 cm⁻¹ and 1325 cm⁻¹ specify the presence of alkane. Absorption at 1617 cm⁻¹ is due to C=C stretching vibration. Absorption at 2916 cm⁻¹ are assigned to aromatic symmetric CH₃ stretching band. Band absorption near 2373 cm⁻¹ corresponds to acid because of the overlapping of C-H. From FTIR results it can be inferred that the bio-organics like triterpenoids, steroids, alcohols, hydrocarbons, Phenolic compounds flavonoids, lignans, coumarins, tannins, quercetin, alkaloids and cynogenic glycosides from Emblica leaves formed a strong capping on the nanoparticles.

3.1.3. Scanning Electron Microscopy

The morphology and structure of the samples were determined using a scanning electron microscope. Fig. 3 shows the scanning electron microscope micrograph of homogeneous ZnO nanorod synthesized using aqueous leaf extract of *Emblica officinalis* free of agglomeration.

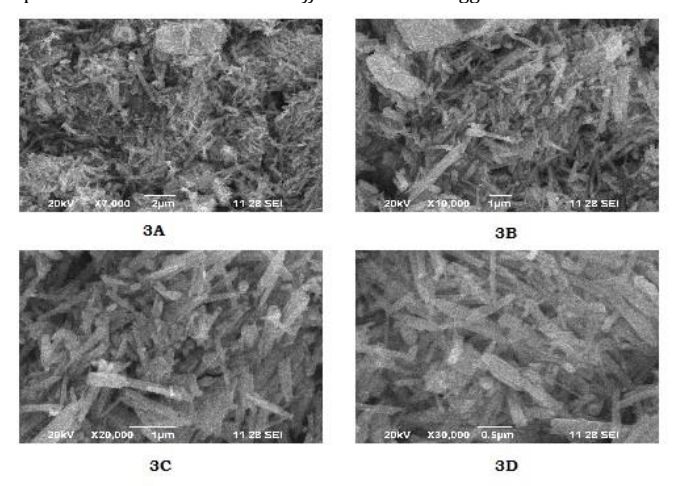


Fig. 3 3A, 3B, 3C and 3D representative SEM image of ZnO-NPs-AS-Eo

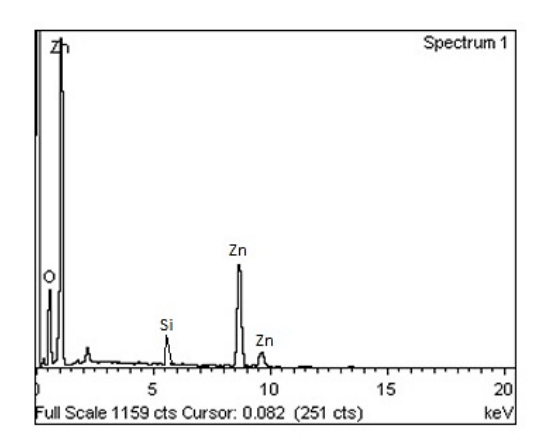


Fig.4 The Elemental Spectra of ZnO-NPs-AS-Eo

3.1.4. Energy Dispersive X-Ray Spectroscopy

The elemental distribution of ZnO nano rods was determined with EDX analysis. EDX spectrum reveals the (Fig. 4) the presence of zinc, oxygen and silicon which is in good agreement with the results of FT-IR and XRD. Owing to this reason the progress of green chemistry with the use of plants in the synthesis of green adsorbent has engrossed a great attention.

3.2. Biosorption Studies

3.2.1. Effect of Dosage and pH

The adsorbent dosage serves as an important parameter in adsorption process, this is because it determines the capacity of an adsorbent for a given initial concentration from the adsorbent. The batch experimental result revealed that the effect of adsorbent dosage on the percentage of As(III) ions removal was observed for adsorbent dosage of 0 to 8 g. The effect of zinc oxide nanoparticle embedded onto activated silica on As(III) adsorption was studied at pH of 0 to 8, 0.02 N initial ion concentration of As(III) ions, contact time of 100 min and agitation speed of 400 rpm. The rate of adsorption increases from 60 to 90 percentages. Further increases of adsorbent amount beyond 8 g/L do not affect the adsorption significantly this observation can be explain in terms of availability of active sites on the adsorbent surface. The graph of percentage removal of As(III) versus pH and initial adsorbent dosage was represented in 3D plots as represented in Fig. 5.

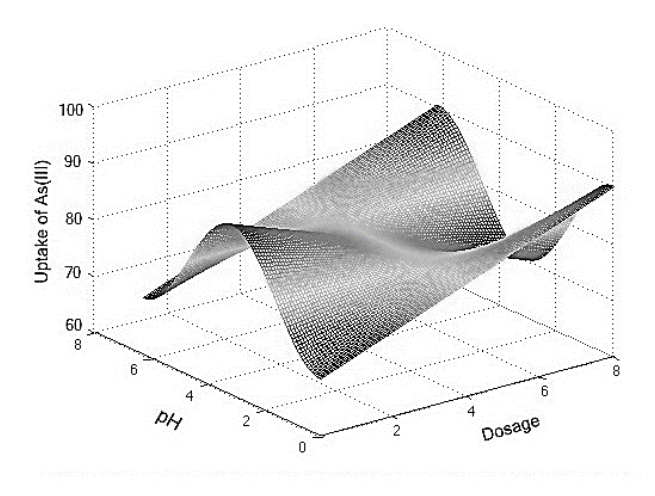


Fig. 5 Percentage removal of As(III) versus pH and initial adsorbent dosage was represented in 3D Plots

3.2.2. Effect of Agitation Speed and pH

The effect of agitation speed rate on As(III) adsorption is shown in Fig. 6 and it appears agitation speed has pronounced effect on the amount As(III) adsorbed. As the agitation speed increased from 100 to 500 rpm, the percentage removal increased from 50.5 % to 97.56 %. However beyond 500 rpm, the adsorption percentage remained constant and the agitation speed of 500 rpm was selected in subsequent analysis. The increase in adsorption capacity at a higher agitation speed could be explained in terms of the reduction of boundary layer thickness around the adsorbent particles. The graph of percentage removal of As(III) versus agitation speed and initial pH was represented in 3D plots as represented in Fig. 6.

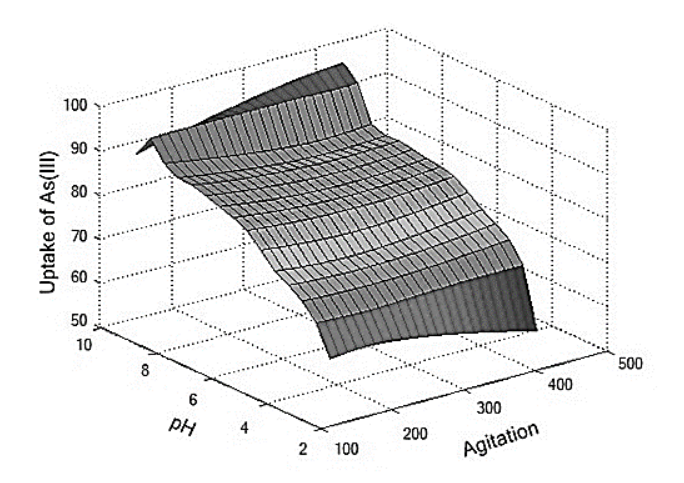


Fig. 6 Percentage removal of As(III) versus pH and a gitation was represented in 3D Plots

3.2.3. Effect of Concentration and Contact Time

The principal driving force for overcoming the total mass transfer resistance of As(III) ion between the solid phase and aqueous phase is the initial metal ion concentration. Effect of initial concentration of As(III) ion was determined by mixing 1 g of adsorbent with 20 mL solution. The contact time was varied in the range 20 - 100 minutes between the adsorbate and adsorbent to study the time dependent behavior of adsorption of As(III) on zinc oxide nanoparticle embedded onto activated silica. The initial concentration of As(III) was kept at 0.02 N, agitation speed at 400 rpm and zinc oxide nanoparticle embedded onto activated silica was 8 g at pH 5.0. The result showed that the percentage removal of As(III) increased when agitation time was increased and equilibrium was reached after 100 minutes. The adsorption of As(III) on zinc oxide nanoparticle embedded onto activated silica was found to be fast at the beginning and become slower as the contact time was increased until the equilibrium reached. The adsorption rate increased from 50 % to 95% and become constant after 100 minutes when the system reached equilibrium. The graph of percentage removal of As(III) versus contact time and concentration was represented in 3D plots as represented in Fig. 7.

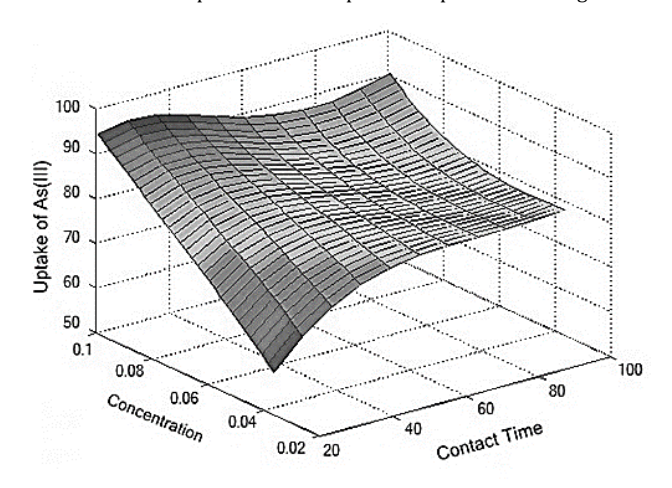


Fig. 7 Percentage removal of As(III) versus concentration and contact time was represented in 3D Plots

3.4. Optimization of the ANN Structure

Fig. 8 shows a feed forward back propagation (FFBP) algorithm with five dependant variables of three-layer architecture a single hidden layer with a tangent sigmoid transfer function (tansig) at input and a linear transfer function (purelin) at output layer are used and run on nftool MATLAB 11a. The distribution of output of training data was presented in (Figs. 8 and 9). At initial stage, 5 neuron was chosen in the hidden layer. With the increase of neuron numbers the MSE value was found decreasing. MSE values was much higher for 5 (MSE= 74.06) and 15 (MSE=37.42) neurons in the hidden layer. With the increase of hidden neurons from 5 to 15, the MSE value decreases from (74.06 to 37.4). With further increasing of hidden neurons the MSE value decreasing further and reached minimum value (MSE=4.3975) at 20 hidden neurons. Hence the neural network containing 20 hidden neurons was selected as optimum case. As neuron number in the hidden layer was increased to 25, the MSE value was found slightly increased to 9.4. With further increase in neuron numbers in hidden layer resulted a sharp increase in the MSE value.

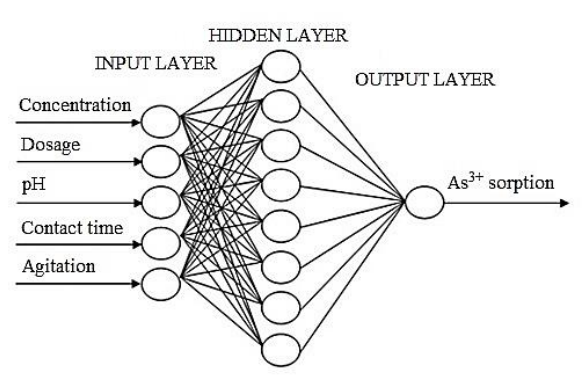


Fig. 8 Predicted ANN architecture for five various parameters.

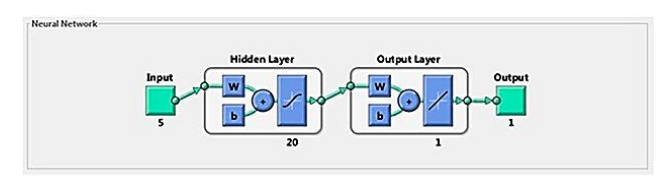


Fig. 9 LMFFBP networks for 5-20-1 type of ANN architecture.

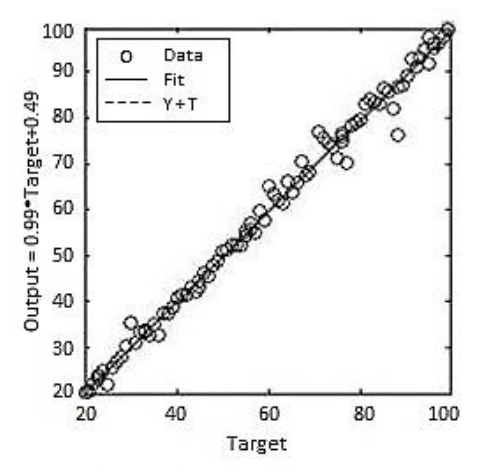


Fig. 10 Regression analysis for adsorption of As(III)

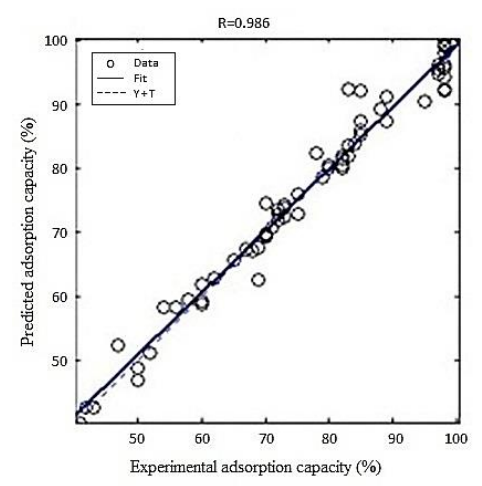


Fig. 11 Comparison between ANN predicted and experimental data

A regression analysis of the network response between ANN outputs and the corresponding targets was performed. The graphical output of the network outputs plotted versus the targets as open circles is illustrated in Fig. 10. Taking into account the non-linear dependence of the data, linear regression shows a good agreement between ANN outputs (predicted data) and the corresponding targets (experimental data). The best linear fit was indicated by a solid red line and R^2 is almost 0.986. The

performance control of ANN outputs was evaluated by estimating the correlation coefficient of 0.99 (Fig. 10).

Fig. 11 shows the relationship between experimental data and BP - ANN model outputs. It can be understood that there is best agreement between calculated and experimental data, which proves that BP - ANN is a most powerful fitting and predictive tool which can describe the adsorption behavior with correlation coefficient of 0.986.

4. Conclusion

In the present study, a three layer feed forward neural network was optimized to predict the As(III) removal efficiency from aqueous solution using zinc oxide nanoparticle embedded onto activated silica as adsorbent. The model consisted of Levenberg-Marquardt back propagation training algorithm with tangent sigmoid transfer function (tansig) between input and hidden layer and linear transfer function (purelin) between hidden and output layer. The MSE value was found lowest (MSE=4.3) at 20 neurons in hidden layer. A regression analysis was performed between model predicted value and experimental data with correlation coefficient (R=0.986) where ANN predicted values are in close agreement (R=0.999) with laboratory batch experimental data. The present studies showed that the ANN model can effectively simulate and predict As(III) removal efficiency in complex adsorption process.

References

- S.V. Flanagan, R.B. Johnston, Y. Zheng, Arsenic in tube well water in Bangladesh: health and economic impacts and implications for arsenic mitigation, Bull. World Health Organ. 90 (2012) 839-846.
- [2] D. Gnanasangeetha, D. Sarala Thambavani, ZnO Nanoparticle Entrenched on Activated silica as a Proficient Adsorbent for Removal of As³⁺, Int. J. Res. Pharm. Biomed. Sci. 4(4) (2013) 1295-1304.
- [3] "Test ID: ASU. Arsenic, 24 Hour, Urine, Clinical Information", Mayo Medical Laboratories Catalog. Mayo Clinic., Retrieved 2012, 09-25.
- [4] P. Muthusamy, S. Murugan, M. Sunitha, Removal of Nickel ion from Industrial waste water using maize cob, ISCA J. Biol. Sci. 1(2) (2012) 7-11.
- [5] W. Saha, K.L. Edwards, The use of artificial neural networks in material science based research, Mater. Des. 28 (2007) 1747-1752.
- [6] A. Abbas, N. Al-Bastaki, Modeling of an RO water desalination unit using neural network, Chem. Eng. J. 114 (2005) 139-143.
- [7] A. Shahavand, M. Pourafshari Chenar, Neural network modeling of hollow fiber membrane processes, J. Membr. Sci. 297 (2007) 59-73.
 [8] D. Gnanasangeetha, D. Sarala Thambavani, Benign ZnO Nanoparticle as a
- [8] D. Gnanasangeetha, D. Sarala Thambavani, Benign ZnO Nanoparticle as a practical Adsorbent for Removal of As³⁺ Embedded on Activated silica using *Ocimum Sanctum*, Discovery, 16(46) (2014) 33-41.
- [9] J.A. Hernandez-Perez, M.A. Garcia-Alvarado, G. Trystram, B. Heyd, Neural networks for the heat and mass transfer prediction during drying of cassava and mango, Innovative Food. Sci. Emerg. technol. 5(1) (2004) 57-64.
- [10] P.C. Panchariya, D. Popovic, A. Sharma, Desorption isotherm modelling of black tea using artificial neural networks, Drying Technol. 20(2) (2002) 351-362.
- [11] D. Gnanasangeetha, D. Sarala Thambavani, Modelling of As³⁺ adsorption from aqueous solution using Azadirachta indica by artificial neural network, Desalin. Water Treat. (2014) 1-16, (doi: 10.1080/19443994.2014.956345)
- [12] S. Janjai, P. Intawee, K. Tohsing, B. Mahayothee, B.K. Bala, M.A. Ashraf, J. Muller, Neural network modeling of sorption isotherms of longan (Dimocarpus longan Lour.), Comp. Elect. Agri. 66(2) (2009) 209-214.
- [13] M. Al-Abri, N. Hilal, Artificial neural network simulation of combined humic substance coagulation and membrane filtration, Chem. Engg. J. 141(1) (2008) 27-34.
- [14] W. Ciezak, Z. Siwon, J. Ciezak, Application for the prediction of time series of short-lived water intake in selected water mains, Ochrona Srodowiska 28(1) (2006) 39-44.